Biosensors and Bioelectronics 25 (2010) 1663–1668

Contents lists available at ScienceDirect

Biosensors and Bioelectronics

journal homepage: www.elsevier.com/locate/bios

Biosensor based on hydrogel optical waveguide spectroscopy

Yi Wang[a], Chun-Jen Huang[a], Ulrich Jonas[b,c], Tianxin Wei[d], Jakub Dostalek[a,*], Wolfgang Knoll[a]

[a] Austrian Institute of Technology, Donau-City-Strasse 1, 1220 Vienna, Austria
[b] Max Planck Institute for Polymer Research, Ackermannweg 10, 55128 Mainz, Germany
[c] FORTH/IESL, Voutes Str. 1527, 71110 Heraklion, Greece
[d] Institute for Chemical Physics, Beijing Institute of Technology, Beijing 100081, People's Republic of China

ARTICLE INFO

Article history:
Received 23 September 2009
Received in revised form
13 November 2009
Accepted 2 December 2009
Available online 11 December 2009

Keywords:
Optical waveguide spectroscopy
Surface plasmon resonance
Hydrogel
Label-free detection
Biosensor

ABSTRACT

A novel label-free biosensor based on the measurement of binding-induced refractive index changes by hydrogel optical waveguide spectroscopy (HOWS) is reported. This biosensor is implemented by using a surface plasmon resonance (SPR) optical setup in which a carboxylated poly(*N*-isoproprylacrylamide) (PNIPAAm) hydrogel film is attached on a metallic surface and modified by protein catcher molecules through amine coupling chemistry. The swollen hydrogel with micrometer thickness serves both as a binding matrix and optical waveguide. We show that compared to regular SPR biosensor with thiol self-assembled monolayer (SAM), HOWS provides an order of magnitude improved resolution in the refractive index measurements and enlarged binding capacity owing to its low damping and large swelling ratio, respectively. A model immunoassay experiment revealed that HOWS allowed detection of IgG molecules (molecular weight 150 kDa) with a 10 pM limit of detection that was 5-fold lower than that achieved for SPR with thiol SAM. For the high capacity hydrogel matrix, the affinity binding was mass transport limited. Therefore, we envisage that HOWS will provide further improved detection limit for low molecular weight analytes or for assays employing lower affinity catcher molecules.

1. Introduction

Rapid and sensitive detection of chemical and biological analytes becomes increasingly important in areas such as medical diagnostics, food control and environmental monitoring. Among various technologies, optical biosensors allowing direct detection of target analytes without the need of additional labels are pushed forward for the applications in these areas (Fan et al., 2008; Gauglitz, 2005). Up to now, a wide range of refractometric-based biosensor platforms relying on the measurement of molecular binding-induced refractive index changes were developed including surface plasmon resonance (SPR) (Liedberg et al., 1983), grating-coupled integrated optical waveguides (grating coupler) (Clerc and Lukosz, 1997; Tiefenthaler and Lukosz, 1989), spectroscopy of leaky dielectric waveguides (resonant mirror) (Buckle et al., 1993; Skivesen et al., 2007; Zourob et al., 2005) and integrated optical Mach–Zehnder interferometer (Heideman and Lambeck, 1999). These devices typically comprise a metallic or dielectric layer structure supporting an optical guided wave that probes the binding of target molecules contained in a sample to catcher molecules immobilized on a sensor surface. The molecular binding events are detected through the induced variations in the characteristics of the optical guided wave. The catcher molecules can be immobilized by using two-dimensional surface architectures such as those based on self-assembled monolayers (SAM) (Jung et al., 2000; Knoll et al., 1996, 2000) or in three-dimensional matrices based on polymers (Lofas and Johnsson, 1990; Lofas et al., 1995) or inorganic nanoporous dielectric films (Rong et al., 2008). Three-dimensional hydrogel binding matrices in which catcher molecules are attached to flexible polymer chains offer an increased sensor response to the affinity binding of target molecules owing to the larger binding capacity and lower steric hindrance compared to the two-dimensional surface architectures.

Recently, carboxylated photocrosslinkable hydrogel polymer networks based on poly(*N*-isopropylacrylamide) (PNIPAAm) and dextran copolymers were synthesized in our laboratory for high capacity binding matrices in surface plasmon resonance (SPR) and surface plasmon-enhanced fluorescence spectroscopy (SPFS) biosensors (Aulasevich et al., 2009; Beines et al., 2007; Knoll et al., 2008; Wang et al., 2009). These hydrogels highly swell in aqueous environment and form stable films with thicknesses up to several micrometers. If attached to a metallic surface, these films can serve as optical waveguides which exhibit more than an order of magnitude lower damping than surface plasmons (Beines et al., 2007; Kuckling and Pareek, 2008). In this paper, we show that the hydrogel optical waveguide spectroscopy (HOWS) allows monitoring the variations of refractive index on the sensor surface with greatly increased accuracy compared to regular SPR. Moreover, a

* Corresponding author. Fax: +43 50550 4399.
E-mail address: jakub.dostalek@ait.ac.at (J. Dostalek).

0956-5663/$ – see front matter © 2009 Elsevier B.V. All rights reserved.
doi:10.1016/j.bios.2009.12.003

thin hydrogel film can serve both as a waveguide and as an affinity binding matrix and thus it provides full overlap of the electromagnetic field of a probing wave with the region where molecular binding events occur. The performance of HOWS is characterized by means of a refractometric study and its implementation for label-free biosensing is demonstrated through a model immunoassay experiment. The obtained results are compared to those measured by regular SPR biosensor relying on thiol SAM surface architecture.

2. Materials and methods

2.1. Materials

All reagents were used as received without further purification. Mouse immunoglobulin G (IgG) and goat anti-mouse immunoglobulin G (a-IgG) were obtained from Invitrogen (Camarillo, CA). 1-Ethyl-3-(3-dimethylaminopropyl)carbodiimide (EDC) and *N*-hydroxysuccinimide (NHS) were from Pierce (Rockford, USA). Phosphate buffered saline (PBS, 140 mM NaCl, 10 mM phosphate, 3 mM KCl, and a pH of 7.4) was purchased from Calbiochem (Darmstadt, Germany). 10 mM acetate buffer (ACT), pH 4, was prepared with sodium acetate and acetic acid by adjusting the pH with HCl and NaOH. Series of buffers with pH between 4 and 7 were prepared by adding HCl or NaOH to a solution of 1.25 mM citric acid, 1.25 mM potassium dihydrogen phosphate, 1.25 mM dipotassium phosphate, 1.25 mM tris-(hydroxymethyl)-aminomethane hydrochloride and 1.25 mM potassium chloride. PBS-Tween buffer (PBST) was prepared by adding Tween 20 (0.05%) in PBS buffer solution. Dithiolaromatic PEG6-carboxylate (thiol-COOH) and dithiolaromatic PEG3 (thiol-PEG) were purchased from SensoPath Technologies (Bozeman, USA). Sodium para-tetrafluorophenol-sulfonate (TFPS) and S-3-(benzoylphenoxy)propyl ethanthioate (thiol-benzophenone) were synthesized at the Max Planck Institute for Polymer Research in Mainz, Germany as described in the literature (Beines et al., 2007; Gee et al., 1999). All the other chemicals were purchased from Sigma–Aldrich (Schnelldorf, Germany).

2.2. Surface architecture

The synthesis and deposition of the PNIPAAm hydrogel that is composed of the terpolymer with *N*-isoproprylacrylamide, methacrylic acid, and 4-methacryloyl benzophenone were performed in our laboratories, as described elsewhere (Beines et al., 2007). Briefly, a thin hydrogel film was spin-coated (from an ethanol solution with polymer dissolved at the concentration of 20 mg mL^{-1}) on a sensor chip surface with thin gold layer that was modified by a thiol-benzophenone SAM. Afterwards, the polymer film was dried overnight in vacuum at 50 °C followed by irradiation with UV light (λ = 365 nm, irradiation dose of 2 J cm^{-2}) in order to cross-link and attach the polymer chains to the gold surface via benzophenone units. The immobilization of mouse IgG catcher molecules in the PNIPAAm hydrogel matrix was performed *in situ*. Firstly, the hydrogel was swollen in ACT buffer and the hydrogel carboxylic moieties were activated by 20 min incubation in water solution with a mixture of TFPS (10.5 mg mL^{-1}) and EDC (37.5 mg mL^{-1}). Then, the surface was rinsed with ACT buffer for 5 min and mouse IgG dissolved in ACT buffer at a concentration of 50 μg mL^{-1} was flowed over the activated hydrogel film for 90 min. After the reaction of mouse IgG with TFPS-activated carboxylic groups, the un-reacted TFPS ester moieties were blocked by 20 min incubation in a solution with 1 M ethanolamine at pH 8.5. Finally, the functionalized hydrogel was successively washed with ACT and PBST buffers for 5 and 10 min, respectively. For comparison, a regular SPR sensor chip with a thin gold layer and mouse IgG molecules immobilized by using a mixed thiol SAM was used. The thiol SAM was formed on a gold surface during overnight incubation in a mixture of thiol-COOH and thiol-PEG (ratio of 1:9) dissolved in absolute ethanol at a total concentration of 0.5 mM. Afterwards, the gold surface was rinsed with ethanol and activated with EDC (37.5 mg mL^{-1}) and NHS (10.5 mg mL^{-1}) solution, and the mouse IgG molecules were immobilized similarly as described for the hydrogel binding matrix. In a control experiment, the carboxylic moieties of the hydrogel film and the SAM were activated as described above and directly deactivated with ethanolamine without binding of IgG molecules.

2.3. Spectroscopy of hydrogel waveguide modes

The HOWS biosensor was implemented by using an optical setup depicted in Fig. 1. A light beam emitted from a stabilized He–Ne laser (25-STP-912-230 from CVI, USA, with a power of 2 mW at a wavelength of λ = 633 nm and 1/e^2 divergence of 0.17°) passed through a polarizer to select transversal magnetic (TM) polarization and was coupled to a high refractive index LASFN9 glass prism (90°, refractive index n_p = 1.845) with a sensor chip optically matched to its base. The sensor chip consisted of a glass slide coated with a gold layer (thickness between 37 and 45 nm) and a PNIPAAm hydrogel film. A cell with the volume 10 μL, length L = 10 mm and depth h = 0.1 mm was pressed against the sensor chip surface to flow liquid samples over the sensor surface at the flow rate of 200 μL min^{-1}. For the comparison study, the regular SPR sensor chip with 45 nm gold and thiol SAM was loaded to the sensor. The assembly of the prism, sensor chip and flow-cell was mounted on a rotation stage (2-circle 414 with the precision 10^{-3} deg, from Huber AG, Germany) to control the angle of incidence of a laser beam θ (measured outside the prism, see Fig. 1). The intensity of the laser beam reflected at the sensor surface was measured by using a photodiode connected to a lock-in amplifier (Model 5210, Princeton Applied Research, USA, integration time 3 s). The reflectivity signal R was determined as a ratio of light intensity reflected from a sensor chip and from a reference blank glass slide. The variations in the reflectivity signal R were acquired with a typical standard deviation $\sigma(R)$ between 7×10^{-5} and 2×10^{-4}.

The evanescent field of a laser beam that is totally internally reflected at the sensor surface penetrates through the gold layer and can couple to surface plasmon (SP) and hydrogel waveguide (HW) modes propagating along the outer metal interface. As Fig. 1 shows, the excitation of SP and HW modes is manifested as two distinct dips in the angular reflectivity spectrum. These dips are located at angles θ for which the propagation constant of the mode β matches the component of the reflected laser beam propagation constant that is parallel to the interface:

$$k_0 n_p \sin\theta = \mathrm{Re}\{\beta\}, \tag{1}$$

where $k_0 = 2\pi/\lambda$ is the light propagation constant in vacuum. The propagation constant β of SP and HW can be determined from the dispersion relation:

$$\tan \kappa d_h = \frac{\gamma_b n_h^2/\kappa n_b^2 + \gamma_m n_h^2/\kappa n_m^2}{1 - (\gamma_b n_h^2/\kappa n_b^2)(\gamma_m n_h^2/\kappa n_m^2)}, \tag{2}$$

in which n_m is the refractive index of the metal, n_b is the refractive index of the analyzed dielectric medium (air or buffer) and $\kappa^2 = (k_0^2 n_h^2 - \beta^2)$, $\gamma_m^2 = (\beta^2 - k_0^2 n_m^2)$, and $\gamma_b^2 = (\beta^2 - k_0^2 n_b^2)$ are the transverse propagation constants in the hydrogel film, the metal and the analyzed medium, respectively. Further, the resonance coupling angle for HW mode is noted as θ_{HW} and the one for surface plasmons as θ_{SP}. Both coupling angles increase when increasing the refracting index of the dielectric adjacent to the gold surface n_h. In the further time resolved experiments, the angle of incidence θ

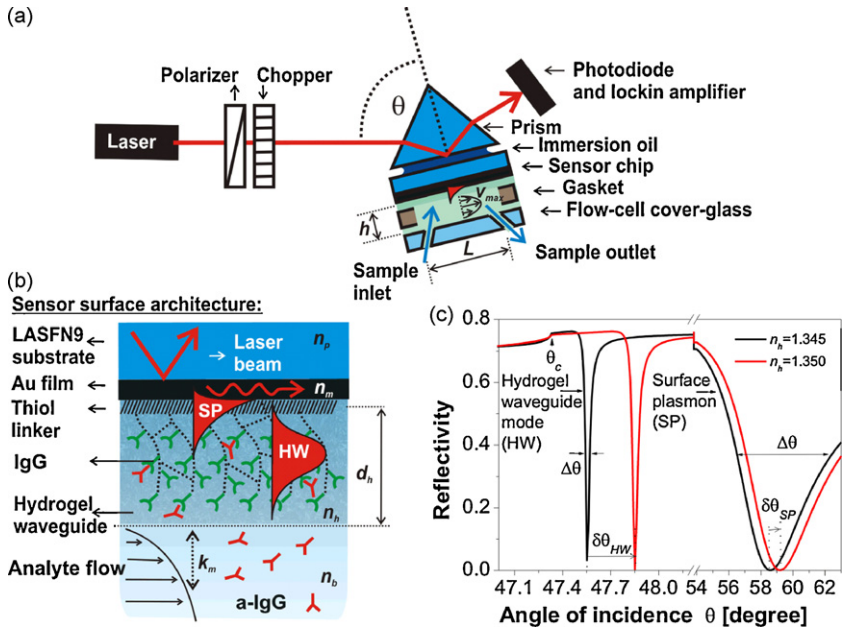

Fig. 1. (a) Optical setup for the excitation of hydrogel waveguide (HW) and surface plasmon (SP) modes, (b) scheme of the sensor surface architecture and (c) simulated changes in the angular reflectivity spectra for the resonant excitation HW and SP modes due to the refractive index increase $\Delta n_h = 5 \times 10^{-3}$ for a hydrogel film with the thickness $d_h = 1.7$ μm and refractive index $n_h = 1.345$.

was set to the location with highest slope $\partial R/\partial\theta$ at the edge of the HW or SP reflectivity dip below the resonant angles θ_{HW} and θ_{SPR}, respectively. A shift in the resonant dips due to the refractive index variations δn_h was measured from induced changes in the reflected intensity δR. In order to determine the thickness d_h and the refractive index n_h of the hydrogel film binding matrix, the angular reflectivity spectrum exhibiting SP and HW resonance dips was fitted by transfer matrix-based model (implemented in the software Winspall developed at the Max Planck Institute for Polymer Research in Mainz, Germany). Similar to our previous investigation (Aulasevich et al., 2009), we assumed a constant refractive index of the gel n_h perpendicular to the surface from which the gel surface mass density was calculated as $\Gamma = (n_h - n_b)d_h\partial c/\partial n_h$, where n_b is the refractive index of buffer and d_h is the thickness of hydrogel. The refractive index of the hydrogel layer was assumed to change with the concentration of the captured protein molecules and with the PNIPAAm polymer chains as $\partial n_h/\partial c = 0.2\ \mathrm{mm^3\ mg^{-1}}$. The diffusion rate k_m of molecules contained in a sample to the sensor surface was estimated by using the two compartment model (Edwards et al., 1999). For a flow-cell with the depth h and length L through which a sample flows with the maximum velocity v_{max}, the diffusion rate k_m can be expressed as:

$$k_M \approx 1.378\left(\frac{v_{max}D^2}{hL}\right)^{1/3}, \quad (3)$$

where D is the diffusion constant of the analyte in a sample. The diffusion constant for the IgG protein in water of $D = 2 \times 10^{-5}\ \mathrm{mm^2\ s^{-1}}$ was assumed (Stepamel et al., 2006).

3. Results and discussion

3.1. Characterization of hydrogel thin film

Firstly, a hydrogel film attached to the gold surface was characterized by the spectroscopy of HW and SP modes. The angular reflectivity spectra $R(\theta)$ were measured for a hydrogel film in contact with air and after its swelling in PBS (see supplement information). By fitting the two distinct resonances at $\theta_{HW} = 21.9°$ and $\theta_{SP} = 76°$ that are associated with the excitation of HW and SP modes in a dry polymer layer, respectively, its thickness $d_h = 230$ nm and refractive index $n_{h\text{-}dry} = 1.48$ was determined. After the swelling in PBS buffer, the HW and SP coupling angles shifted to $\theta_{HW} = 47.75°$ and $\theta_{SP} = 58.20°$, respectively. The fitting of corresponding reflectivity spectrum revealed that the thickness of the swollen gel increased to $d_h = 1.86$ μm and the refractive index decreased to $n_h = 1.3454$. This refractive index is very close to that of the PBS buffer $n_b = 1.3340$ and it corresponds to the polymer volume fraction of 8% and swelling ratio 12.5 as estimated by using the effective medium theory (Ghosh and Pal, 2007). Let us note that for the HOWS the thickness of the hydrogel film needs to be higher than so called cut-off thickness (typically $d_h > 1$ μm) below which the hydrogel waveguide modes cease to exist.

3.2. Refractometric study of HOWS sensor

A refractometric study was performed in order to compare the accuracy with which the refractive index changes on the sensor surface can be measured by HOWS and SPR. In this experiment, changes in the reflectivity spectra were measured upon flowing a series of liquid samples with increasing n_b. These samples were prepared by spiking the PBS buffer ($n_b = 1.3334$) with ethylene glycol (refractive index $n = 1.4314$) at concentrations between 0% and 8% (refractive index changes linear with the concentration of EG with the slope $\delta n_b = 9.8 \times 10^{-4}$ RIU per % at the wavelength $\lambda = 633$ nm and room temperature). As seen in Fig. 2a, resonant dips associated with the excitation of HW and SP modes shift towards higher angles of incidence when the refractive index n_b of a liquid at the sensor surface increases. The fitting of the measured reflectivity spectra with a transfer matrix-based model revealed that the hydrogel thickness d_h was between 1.86 and 1.91 μm and its index n_h linearly increased with the bulk refractive index of the sample with a slope of $\partial n_h/\partial n_b = 0.89$. These results indicate that approximately 90% of the hydrogel volume was accessible for EG molecules diffusing from the aqueous phase into the hydrogel film which is in agreement with the lower maximum shift of HW resonance angle (0.64°) compared to the corresponding critical angle shift (0.68°) (see Fig. 2a). The sensitivity to bulk refractive index changes δn_b was determined

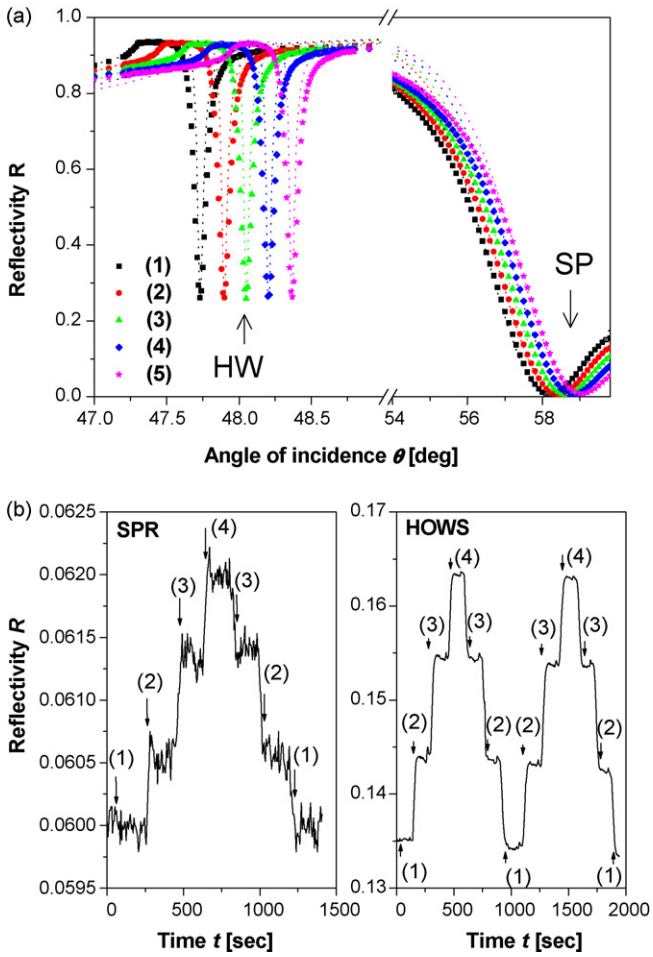

Fig. 2. (a) Measured angular reflectivity spectra for a hydrogel waveguide film in contact with PBS buffer spiked with ethylene glycol (EG) at the concentration from (1) 0%, (2) 2%, (3) 4%, (4) 6% and (5) 8%. The fitted spectra are shown as dotted line. (b) Comparison of the time evolution of the sensor signal measured by SPR and HOWS upon the successive injections of the PBS buffer spiked with EG at concentrations of (1) 0.125%, (2) 0.25%, (3) 0.375% and (4) 0.5%.

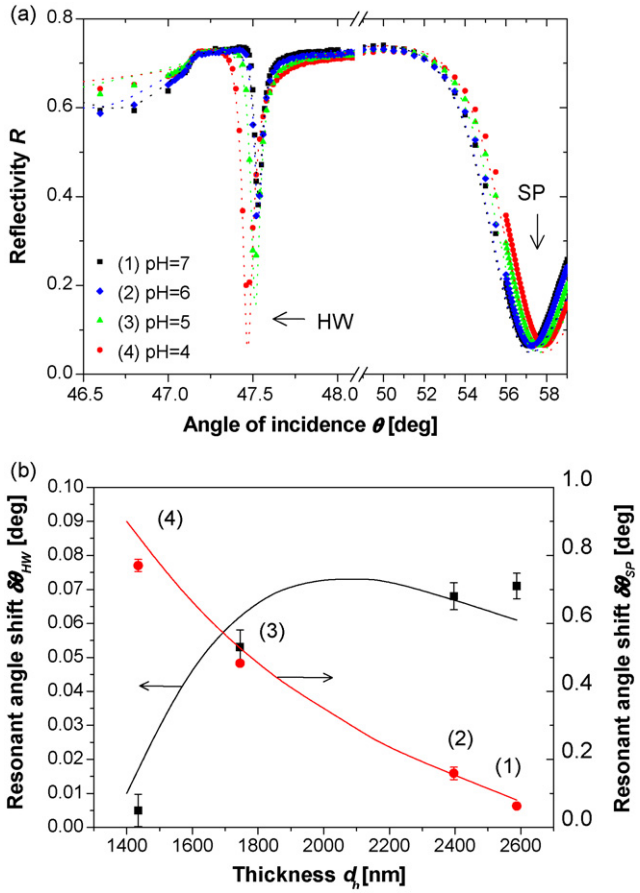

Fig. 3. (a) Angular reflectivity spectra for a hydrogel film measured in buffer with pH value of (1) 7, (2) 6, (3) 5 and (4) 4. (b) The dependence of the resonance angle for the excitation of HW and SP modes on the thickness of the hydrogel observed experimentally (dots) and obtained from transfer matrix-based simulations (line).

as $S = \delta\theta/\delta n_b$, where $\delta\theta$ is the angular shift of the reflectivity dip. The HOWS exhibited a sensitivity of $S = 81^\circ\,\mathrm{RIU}^{-1}$ that is 1.3-fold lower than the one measured for SPR $S = 106^\circ\,\mathrm{RIU}^{-1}$. However, the full width in the half minimum (FWHM) of the HW resonance dip was of $\Delta\theta = 0.1^\circ$ which is approximately 50-fold lower compared to that of the SP dip of $\Delta\theta = 5.1^\circ$. In refractometric sensors based on spectroscopy of guided waves, the figure of merit defined as $\chi = S/\Delta\theta$ is inversely proportional to the resolution with which the refractive index variations can be measured (Homola et al., 1999). By comparing the figure of merit of HOWS ($\chi = 810$) with that of SPR ($\chi = 20.8$), we estimated that HOWS can allow measurement of the refractive index variations on the sensor surface with an accuracy improved by a factor of about 40 with respect to regular SPR. Fig. 2b shows the time evolution of HOWS and SPR reflectivity signal R measured upon the successive flow of PBS samples spiked with EG at concentrations of 0%, 0.125% ($\delta n_b = 1.23 \times 10^{-4}$ RIU), 0.25% ($\delta n_b = 2.45 \times 10^{-4}$ RIU), 0.375% ($\delta n_b = 3.68 \times 10^{-4}$ RIU) and 0.5% ($\delta n_b = 4.9 \times 10^{-4}$ RIU). These data show that the reflectivity signal changed with a slope of $\partial R/\partial n_b$ of 78 and 5.6 RIU^{-1} for HOWS and SPR-based measurements, respectively, which translated to 10-fold higher refractive index resolution provided by HOWS (1.3×10^{-6} RIU) compared to that of SPR (1.3×10^{-5} RIU) (defined as the ratio of standard deviation $\sigma(R)$ and the slope $\partial R/\partial n_b$). This factor is lower than that predicted by the previous comparison of figure of merit due to the lower coupling efficiency to HOW modes and due to the non-symmetrical SPR resonance dip which exhibited higher slope below the resonant angle θ_{SPR} than that above it.

3.3. Sensitivity to swelling changes of HOWS sensor

As shown in previous studies, changes in swelling of PNIPAAMm hydrogel films occur upon the binding of biomolecules (Aulasevich et al., 2009; Wang et al., 2009) as well as due to variations in the ionic strength and pH (Beines et al., 2007; Huang et al., 2009) which may interfere with the response due to the specific capture of target analyte (Xu et al., 2006). In general, the binding of target molecules as well as the swelling variations alter the thickness d_h and consequently refractive index n_h of the hydrogel film leading to a shift of the angular position of resonant dip associated with the excitation of hydrogel waveguide and surface plasmon modes. The sensitivity of HOWS and SPR to swelling changes of a binding matrix was investigated in an experiment in which buffers with pH between 4 and 7 were flowed over the hydrogel film. As seen in Fig. 3a, decreasing the pH causes an increase of the resonant angle θ_{SP} and a decrease of the resonant angle θ_{HW}. The fitting of measured angular reflectivity spectra presented in Fig. 3a revealed that the decrease of pH caused a collapse of the gel upon which the thickness decreased from $d_h = 2600$ nm (pH = 7) to $d_h = 1400$ nm (pH = 4). Let us note that in this experiment the surface mass density of the gel ($\Gamma = 105\,\mathrm{ng\,mm^{-2}}$) did not change upon the swelling and that the increased coupling efficiency observed for HW mode propagat-

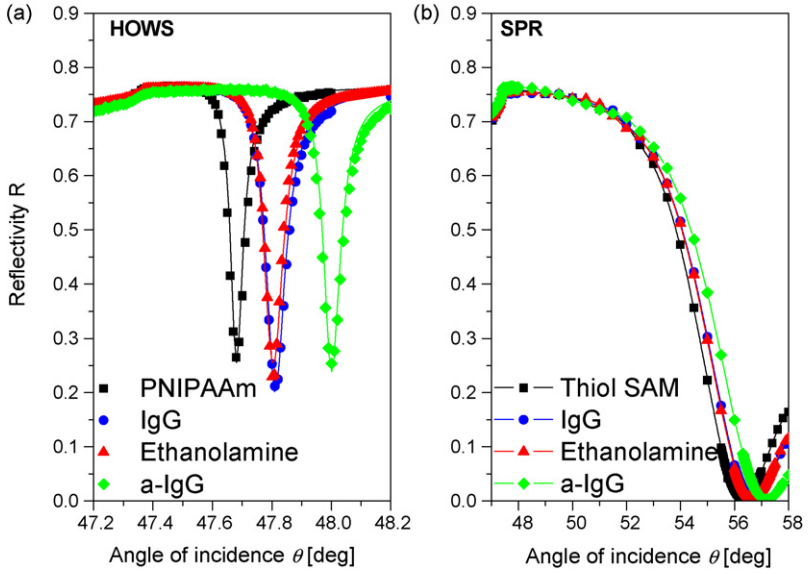

Fig. 4. Angular reflectivity spectra of (a) a hydrogel film and (b) thiol SAM in contact with PBST buffer (black squares), after the immobilization of catcher molecules (blue circles, IgG), incubation in ethanolamine (red triangles) and saturation of affinity binding of analyte molecules (green diamonds, a-IgG), measured by (a) HOWS and (b) SPR, respectively. (For interpretation of the references to color in this figure legend, the reader is referred to the web version of this article.)

ing along the hydrogel film with the lower thickness is caused by a stronger overlap of the field of the excitation incident wave and HW. In Fig. 3b, the experimental dependence of the resonant angles θ_{HW} and θ_{SP} on the thickness of the gel is compared to simulations based on transfer matrix model. These data reveal good agreement between theory and experiment and show that changes in θ_{HW} due to the swelling variations are an order of magnitude lower than those for θ_{SP}. In addition, the simulations show that the derivation $\partial\theta_{HW}/\partial d_h$ can reach zero for the certain thickness d_h which illustrates that the sensitivity of θ_{HW} to small swelling variations can be totally eliminated by a design of the hydrogel binding matrix. This is an important advantage of HOWS as the regular SPR exploiting a three-dimensional binding matrix does not allow distinguishing between the surface mass density and swelling changes.

3.4. Immobilization of catcher biomolecules

In order to demonstrate the application of HOWS for the monitoring of molecular binding events, IgG catcher molecules were firstly immobilized to the PNIPAAm hydrogel. As seen in Fig. 4a, the covalent coupling of IgG to the gel shifted the angular position of the resonant dip from $\theta_{HW} = 47.68^\circ$ to 47.80°. By fitting the changes in the angular reflectivity spectra, we determined that the surface mass density increased due to the loading of IgG molecules in the hydrogel from $\Gamma = 98\,ng\,mm^{-2}$ to $118\,ng\,mm^{-2}$. After the blocking the un-reacted TFPS groups by ethanolamine and rinsing with PBS, the surface mass density decreased to $\Gamma = 114\,ng\,mm^{-2}$. This decrease can be attributed to the release of loosely bound polymer chains and IgG molecules from the hydrogel film. By comparing the surface mass density before and after the loading with IgG molecules, the surface coverage of the immobilized IgG can be estimated as $\Delta\Gamma = 16–20\,ng\,mm^{-2}$. The immobilization of IgG on a gold surface by using thiol SAM with carboxylic moieties resulted in the surface coverage of $\Delta\Gamma = 1.7\,ng\,mm^{-2}$ as determined by the analysis of the angular reflectivity spectra in Fig. 4b.

3.5. Immunoassays-based HOWS biosensing

The affinity binding of a-IgG molecules was observed upon a sequential injection of a series of samples with a-IgG dissolved in PBST at concentrations ranging from 0.6 nM to 0.6 μM. Each sample was flowed over the sensor surface with immobilized catcher molecules for 30 min followed by a 10 min rinsing with PBST buffer. As seen in Fig. 5a, the capture of a-IgG molecules during a sample flow was manifested as a gradual increase in the HOWS and SPR reflectivity signal δR due to the affinity binding-increased refractive index on the surface. In a control experiment, no measurable increase signal δR was observed for a flow of 6 and 60 nM a-IgG over the surfaces that were not modified with IgG molecules. The calibration curve showing the dependence of the reflectivity changes on the concentration of a-IgG in a sample is presented in Fig. 5b. These data reveal that the reflectivity changes δR observed by HOWS were larger compared to SPR and allowed for the detection of a-IgG with 5-fold improved limit of detection (LOD) of 10 pM. The LOD was determined as the concentration for which the calibration curve reaches the three-time standard deviation of reflectivity signal baseline $3\sigma(R)$. To observe the binding capacity of the sensor, a solution with a-IgG molecules at the concentration of 0.6 μM was flowed over the sensor surface until the sensor response was stabilized. The sensor response stabilized much slower for hydrogel binding matrix (the slope $\partial R/\partial t$ decreased 50-fold after 200 min) compared to SPR with monolayer surface architecture (after 17 min). From the induced shifts $\delta\theta_{SPR} = 0.55^\circ$ measured by SPR and $\delta\theta_{HW} = 0.19^\circ$ obtained by HOWS (Fig. 4), the amount of captured a-IgG was determined as 2.6 and $36\,ng\,mm^{-2}$ on the thiol SAM and in the hydrogel, respectively. Let us note that we carried out similar experiment for the hydrogel matrix with SPR readout of a-IgG affinity binding (data not shown), and we observed 5-fold lower angular shift $\delta\theta_{SPR}$ (compared to that in Fig. 4b) owing to the fact that the binding-induced refractive index increase in the gel was compensated by the effect of increased hydrogel swelling (thickness). The HOWS angular shift was too large to be measured by tracking the reflectivity change δR. Therefore, the corresponding reflectivity change was estimated as $\delta R_{HW} = \delta\theta_{HW} \times \partial R/\partial\theta = 1.72$ which is 14.3-fold larger than that measured by SPR of $\delta R_{SPR} = 0.12$. The reason for the slow saturation of the HOWS signal and for only 5-fold improvement of LOD is the slow diffusion of the analyte to the sensor surface. The mass transport coefficient of the a-IgG molecules to the hydrogel surface was calculated as $k_m \sim 3 \times 10^{-3}\,mm\,s^{-1}$ by using Eq. (3). By fitting the measured SPR kinetics $R(t)$ with the Langmuir adsorption model (data not shown), the association rate constant for the

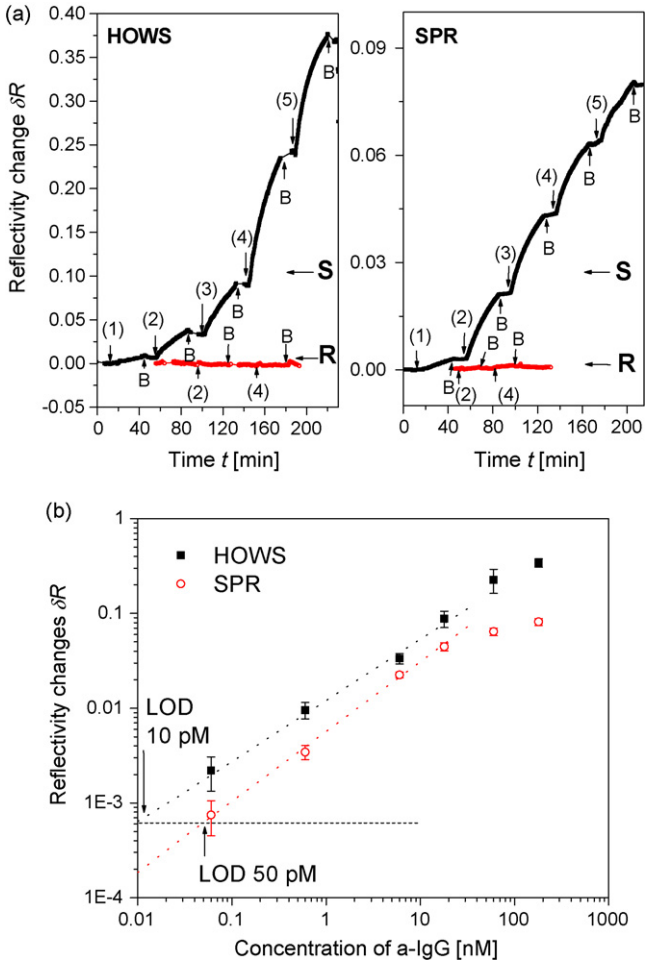

Fig. 5. (a) The time kinetics of the SPR and HOWS reflectivity changes ΔR due to the affinity binding of analyte a-IgG molecules dissolved at the concentration of (1) 0.6, (2) 6, (3) 18, (4) 60 and (5) 180 nM flowed over the sensor surface, modified with IgG catcher molecules (S) and a reference surface without IgG molecules (R). In between injections of samples, the sensor surface was rinsed with PBST buffer (B). (b) The calibration curves for the detection of anti-IgG measured by HOWS (black squares) and SPR (red circles) fitted with linear function (correlation coefficients 0.9913 ($n = 4$) and 0.9961 ($n = 4$), respectively). (For interpretation of the references to color in this figure legend, the reader is referred to the web version of this article.)

a-IgG/IgG pair was estimated as $k_a > 10^5\ M^{-1}\ s^{-1}$. For the receptor surface coverage in the hydrogel of $\Delta\Gamma \sim 1.3 \times 10^{-13}$ mol mm^{-2} (corresponding to IgG surface mass density of $\Delta\Gamma = 20$ ng mm^{-2} determined previously and to the molecular weight of IgG 150 kDa), the affinity binding rate of $k_a\ \Delta\Gamma > 10^{-2}$ mm s^{-1} is obtained that is more than three times higher than k_m and which confirms that the molecular binding was diffusion controlled.

4. Conclusions

A new biosensor for direct label-free detection of molecular analytes based on a three-dimensional hydrogel binding matrix and the spectroscopy of hydrogel waveguide modes was presented. This biosensor was implemented by using an optical setup for angular spectroscopy of guided waves and UV-crosslinkable carboxylated PNIPAAm hydrogel in which catcher molecules were immobilized by amine coupling chemistry. With respect to regular SPR biosensor, HOWS was demonstrated to provide an order of magnitude enhanced resolution in the measurement of refractive index changes, binding capacity, and equilibrium sensor response due to the affinity binding of target molecules. In addition, design of the layer allows to greatly suppress the cross sensitivity of HOWS to effects accompanied with hydrogel swelling changes. For immunoassay-based observation of affinity binding of 150 kDa IgG target molecules, HOWS allowed to reach a 10 pM limit of detection that was improved by a factor of five compared to regular SPR. We expect that HOWS will enable higher sensitivity enhancement for detection of small molecules that can diffuse faster to the surface or for assays that exploit low affinity catcher molecules e.g. for continuous monitoring of target analytes (Ohlson et al., 2000). The future work will include employing more advanced optical schemes and data processing methods for tracking of the angular resonance position (Nenninger et al., 2002). In addition, the presented method can be straightforward extended for multi-analyte and reference-compensated measurements on arrays of sensing spots defined on the sensor chip by crosslinking of the hydrogel by UV through appropriate mask.

Acknowledgements

The authors would like to acknowledge the help of Alena Aulasevich, Martina Knecht and Yameen Basit (Max Planck Institute for Polymer Research) with the synthesis of PNIPAAm hydrogel, S-3-(benzoylphenoxy)propyl ethanthioate and sodium para-tetrafluorophenol-sulfonate. Partial support for this work was provided by the Deutsche Forschungsgemainschaft (KN 224/18-1, Schwerpunktprogramm "Intelligente Hydrogele", SPP 1259) and by the 111 Project (B07012).

Appendix A. Supplementary data

Supplementary data associated with this article can be found, in the online version, at doi:10.1016/j.bios.2009.12.003.

References

Aulasevich, A., Roskamp, R.F., Jonas, U., Menges, B., Dostalek, J., Knoll, W., 2009. Macromol. Rapid Commun. 30, 872–877.
Beines, P.W., Klosterkamp, I., Menges, B., Jonas, U., Knoll, W., 2007. Langmuir 23 (4), 2231–2238.
Buckle, P.E., Davies, R.J., Kinning, T., Yeung, D., Edwards, P.R., Pollardknight, D., Lowe, C.R., 1993. Biosens. Bioelectron. 8 (7–8), 355–363.
Clerc, D., Lukosz, W., 1997. Sens. Actuators B 40 (1), 53–58.
Edwards, D.A., Goldstein, B., Cohen, D.S., 1999. J. Math. Biol. 39 (6), 533–561.
Fan, X.D., White, I.M., Shopoua, S.I., Zhu, H.Y., Suter, J.D., Sun, Y.Z., 2008. Anal. Chim. Acta 620 (1–2), 8–26.
Gauglitz, G., 2005. Anal. Bioanal. Chem. 381 (1), 141–155.
Gee, K.R., Archer, E.A., Kang, H.C., 1999. Tetrahedron Lett. 40 (8), 1471–1474.
Ghosh, S.K., Pal, T., 2007. Chem. Rev. 107 (11), 4797–4862.
Heideman, R.G., Lambeck, P.V., 1999. Sens. Actuators B 61 (1–3), 100–127.
Homola, J., Koudela, J., Yee, S.S., 1999. Sens. Actuators B 54 (1–2), 16–24.
Huang, C.J., Jonas, U., Dostalek, J., Knoll, W., 2009. Proc. SPIE 7356, 735625.
Jung, L., Nelson, K., Stayton, P., Campbell, C., 2000. Langmuir 16 (24), 9421–9432.
Knoll, W., Kasry, A., Yu, F., Wang, Y., Brunsen, A., Dostalek, J., 2008. J. Nonlinear Opt. Phys. Mater. 17 (2), 121–129.
Knoll, W., Liley, M., Piscevic, D., Spinke, J., Tarlov, M., 1996. Adv. Biophys. 34, 231–251.
Knoll, W., Zizlsperger, M., Liebermann, T., Arnold, S., Badia, A., Liley, M., Piscevic, D., Schmitt, F.J., Spinke, J., 2000. Colloid Surf. A 161 (1), 115–137.
Kuckling, D., Pareek, P., 2008. Polymer 49 (6), 1435–1439.
Liedberg, B., Nylander, C., Lundstrom, I., 1983. Sens. Actuators 4 (2), 299–304.
Lofas, S., Johnsson, B., 1990. J. Chem. Soc., Chem. Commun. 21, 1526–1528.
Lofas, S., Johnsson, B., Edstrom, A., Hansson, G., Linquist, G., Muller, R., Stigh, L., 1995. Biosens. Bioelectron. 10 (10), 813–822.
Nenninger, G.G., Piliarik, M., Homola, J., 2002. Meas. Sci. Technol. 13 (12), 2038–2046.
Ohlson, S., Jungar, C., Strandh, M., Madenjus, C.F., 2000. Trends Biotechnol. 18 (2), 49–52.
Rong, G., Najmaie, A., Sipe, J.E., W, S.M., 2008. Biosens. Bioelectron. 23, 1572–1576.
Skivesen, N., Horvath, R., Thinggaard, S., Larsen, N.B., Pedersen, H.C., 2007. Biosens. Bioelectron. 22 (7), 1282–1288.
Stepamel, J., Vaisocherova, H., Piliarik, M., 2006. In: Homola, J. (Ed.), Surface Plasmon Resonance Based Sensors. Springer, Heidelberg, pp. 69–91.
Tiefenthaler, K., Lukosz, W., 1989. J. Opt. Soc. Am. B 6 (2), 209–220.
Wang, Y., Brunsen, A., Jonas, U., Dostalek, J., Knoll, W., 2009. Anal. Chem. 81 (23), 9625–9632.
Xu, F., Persson, B., Lofas, S., Knoll, W., 2006. Langmuir 22 (7), 3352–3357.
Zourob, M., Mohr, S., Brown, B.J.T., Fielden, P.R., McDonnell, M.B., Goddard, N.J., 2005. Biosens. Bioelectron. 21 (2), 293–302.